# Quantum-enhanced sensing on optical transitions through finite-range interactions

https://doi.org/10.1038/s41586-023-06472-z

Received: 17 March 2023

Accepted: 21 July 2023

Published online: 30 August 2023



Johannes Franke<sup>1,2</sup>, Sean R. Muleady<sup>3,4</sup>, Raphael Kaubruegger<sup>2,5</sup>, Florian Kranzl<sup>1,2</sup>, Rainer Blatt<sup>1,2</sup>, Ana Maria Rey<sup>3,4 $\boxtimes$ </sup>, Manoj K. Joshi<sup>2</sup> & Christian F. Roos<sup>1,2 $\boxtimes$ </sup>

The control over quantum states in atomic systems has led to the most precise optical atomic clocks so far<sup>1-3</sup>. Their sensitivity is bounded at present by the standard quantum limit, a fundamental floor set by quantum mechanics for uncorrelated particles, which can-nevertheless-be overcome when operated with entangled particles. Yet demonstrating a quantum advantage in real-world sensors is extremely challenging. Here we illustrate a pathway for harnessing large-scale entanglement in an optical transition using 1D chains of up to 51 ions with interactions that decay as a power-law function of the ion separation. We show that our sensor can emulate many features of the one-axis-twisting (OAT) model, an iconic, fully connected model known to generate scalable squeezing<sup>4</sup> and Greenberger-Horne-Zeilinger-like states<sup>5-8</sup>. The collective nature of the state manifests itself in the preservation of the total transverse magnetization, the reduced growth of the structure factor, that is, spin-wave excitations (SWE), at finite momenta, the generation of spin squeezing comparable with OAT (a Wineland parameter  $^{9,10}$  of  $-3.9 \pm 0.3$  dB for only N = 12 ions) and the development of non-Gaussian states in the form of multi-headed cat states in the Q-distribution. We demonstrate the metrological utility of the states in a Ramseytype interferometer, in which we reduce the measurement uncertainty by  $-3.2 \pm 0.5$  dB below the standard quantum limit for N = 51 ions.

Quantum sensors offer the promise of performing metrological tasks at a level not possible in classical systems by harnessing entanglement<sup>11-13</sup>. Nonetheless, to generate entanglement, interactions are required, which add undesirable complications, particularly when they are short-ranged in nature<sup>14</sup>. From this consideration, sensors offering full connectivity and operating with macroscopic ensembles to enhance the rate and level of achievable entanglement, such as atoms interacting through all-to-all photon-mediated interactions in optical  $cavities, are at present at the frontier of entanglement generation {}^{15-20}. \\$ However, these platforms lack the desired single-particle control in a quantum sensor, given that the size and control of a system are often competing priorities. On the contrary, in platforms in which individual addressing is possible at present, including ultracold molecules<sup>21</sup>, optical lattices or tweezer clocks  $^{14,22}\!$  , interactions between atoms typically decrease with distance, and the ability to engineer all-to-all connectivity is often severely limited. In trapped ions, both single-particle control and all-to-all interactions are available. However, implementing all-to-all interactions in arrays of tens to hundreds of ions<sup>23,24</sup> faces  $technical \, hurdles \, that \, limit \, the \, coherent \, generation \, of \, entanglement.$ 

A possible solution to harnessing metrologically useful entanglement has been proposed with the suggestion that systems exhibiting short-ranged interactions could nonetheless offer an opportunity for generating entanglement for metrological applications at a level comparable with all-to-all interacting systems<sup>25–29</sup>, although such

predictions inherently rely on uncontrolled approximations to the quantum many-body dynamics because exact treatments are not available at present. Here we experimentally validate these predictions by transforming the fragile Ising interactions arising between an optical transition in a string of up to 51 trapped  $^{40}$ Ca $^+$  ions coupled through power-law interactions into an XY model by applying a large transverse drive to our system. In contrast to the Ising model, the XY model features interactions that favour spin alignment and thus can stabilize collective behaviour. We indeed observe that this model enables the survival of features intrinsic to OAT dynamics, including spin squeezing, the development of collective excitations and, at later times in the dynamics, the creation of multi-headed cat states  $^{5-8}$ . Furthermore, we show improved phase-estimation sensitivity in a Ramsey sequence with a string of N=51 ions.

## Setup and theory

Quantum limits in sensing are commonly discussed for collective systems in which all operations act identically on each particle. A characteristic collective interaction is the OAT model, described by the Hamiltonian

$$\hat{H}_{\text{OAT}} = \frac{\chi}{2} \sum_{i < j}^{N} \hat{\sigma}_{i}^{z} \hat{\sigma}_{j}^{z}, \tag{1}$$

<sup>1</sup>Institut für Experimentalphysik, Universität Innsbruck, Innsbruck, Austria. <sup>2</sup>Institut für Quantenoptik und Quanteninformation, Österreichische Akademie der Wissenschaften, Innsbruck, Austria. <sup>3</sup>JILA, NIST and Department of Physics, University of Colorado, Boulder, CO, USA. <sup>5</sup>Institut für Theoretische Physik, Universität Innsbruck, Innsbruck, Austria. <sup>33</sup>e-mail: arey@jila.colorado.edu; christian.roos@uibk.ac.at

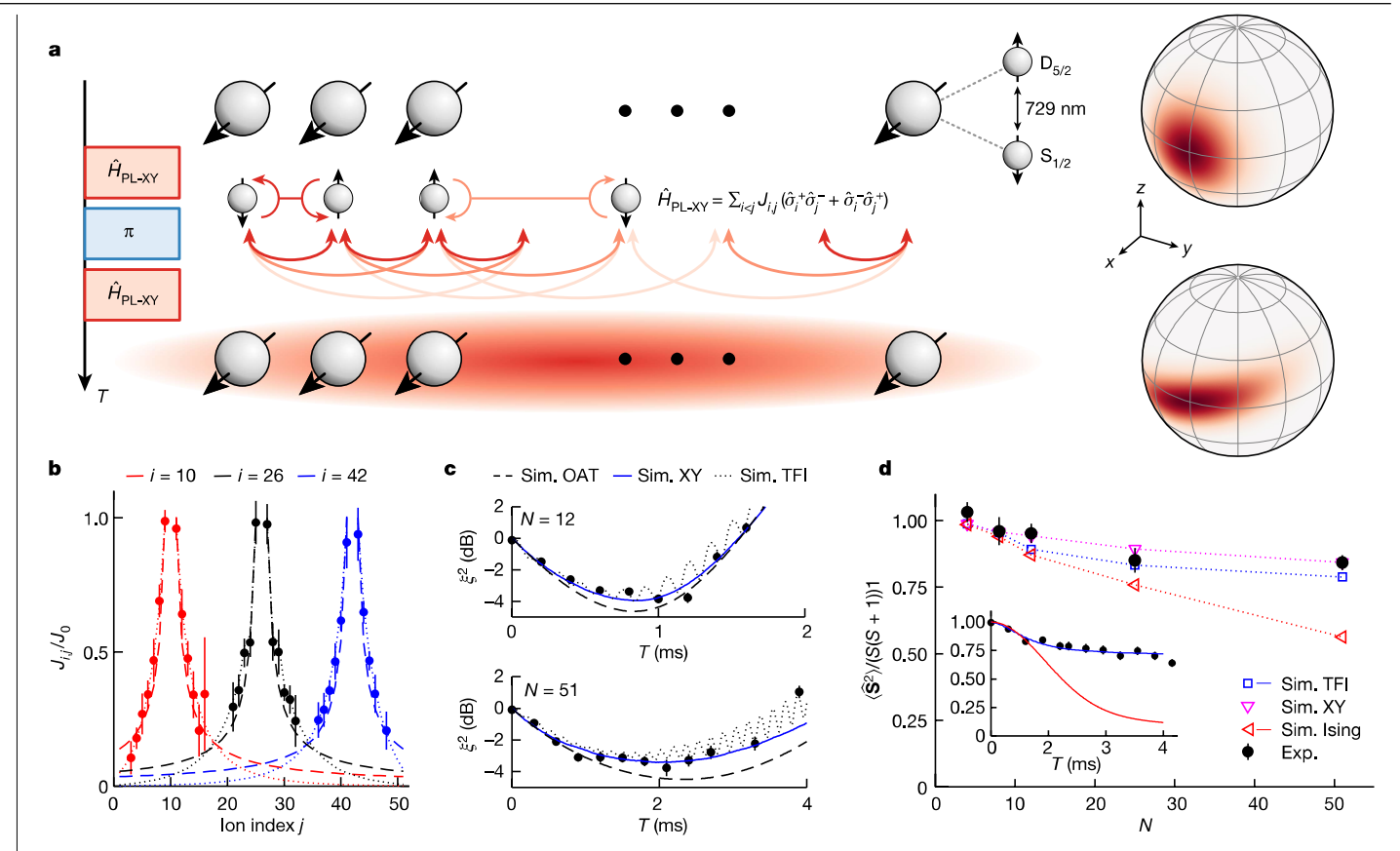


**Fig. 1**| **Realization of squeezing by non-collective interactions. a**, Experimental sequence describing exchange-interaction-induced squeezing of the overall spin vector. We provide a schematic of our ion chain, with qubits encoded on an optical transition. These interact by means of power-law XY interactions, in which the interaction rate decreases with distance. Our sequence combines interaction pulses (red) with pulses from a global addressing beam (blue) to evolve an initial CSS into a SSS, as illustrated on the collective Bloch sphere. **b**, Measured spin–spin couplings  $J_{i,j}$  in a 51-ion chain (dotted line, fit by a power-law interaction with  $\alpha \approx 0.9$ ; dashed line, predicted coupling for the given mode structure and laser detuning). **c**, Measured squeezing versus interaction time for  $\alpha \approx 1, J_0 = 560$  rad s<sup>-1</sup> in a 12-ion chain and  $\alpha \approx 0.9$ ,  $J_0 = 216$  rad s<sup>-1</sup> in a 51-ion chain. We compare with numerical calculations of the dynamics for the corresponding XY model (solid blue line) and dynamics

in the presence of a finite transverse field (dotted black line; see Methods section 'Numerical methods'), as well as theoretical results for the OAT model (dashed black lines), all taking into account our measured decoherence. **d**, Total spin, measured at the time at which the spin-squeezing peaks in the XY model (interaction strength between 216 and 234 rad s<sup>-1</sup> for all system sizes N) and normalized by its maximal value S(S+1) for S=N/2. We compare with numerical simulations with (blue squares) and without (magenta downward-pointing triangles) a finite transverse field and with analytic results for the Ising model after the same evolution time (red left-pointing triangles). The inset shows the total spin as a function of interaction time T for S1 ions compared with theoretical results for the Ising models without (red line) and with (blue line) transverse field.

in which we define Pauli operators  $\hat{\sigma}^x = \hat{\sigma}^+ + \text{h.c.}$  and  $\hat{\sigma}^y = -i(\hat{\sigma}^+ - \text{h.c.})$  with  $\hat{\sigma}^+ = |\uparrow\rangle\langle\downarrow|$  and  $\hat{\sigma}^z = |\uparrow\rangle\langle\uparrow| - |\downarrow\rangle\langle\downarrow|$ . The corresponding collective spin operators are  $\hat{S}_\mu = \sum_i \hat{\sigma}_i^\mu/2$ ,  $\mu = x, y, z$ .

Starting from an initial uncorrelated coherent spin state (CSS) with all spins polarized along  $+x \mid \mathbf{x} \rangle = \bigotimes_{i=1}^N \mid + \rangle_i$  and  $\mid + \rangle = (\mid \uparrow \rangle + \mid \downarrow \rangle)/\sqrt{2}$ , the OAT Hamiltonian shears the classical noise distribution and transforms it into a spin-squeezed state (SSS). The presence of spin squeezing in the resulting state can be quantified through the Wineland parameter, defined as  $^{9.10}$ 

$$\xi^2 = \frac{N\langle (\Delta \hat{S}_{\mathbf{n}_{\perp}})^2 \rangle}{|\langle \hat{\mathbf{S}} \rangle|^2},\tag{2}$$

in which  $\mathbf{n}_{\perp}$  is the axis of minimum variance  $\langle (\Delta \hat{S}_{\mathbf{n}_{\perp}})^2 \rangle \equiv \langle (\hat{S}_{\mathbf{n}_{\perp}} - \langle \hat{S}_{\mathbf{n}_{\perp}} \rangle)^2 \rangle$  transverse to the Bloch vector  $\langle \hat{\mathbf{S}} \rangle$ . This parameter witnesses entanglement when  $\xi^2 < 1$  and quantifies the metrological gain in phase sensitivity,  $\Delta \phi$ , to a collective rotation over that achieved by an initial uncorrelated state,  $\Delta \phi_{\mathrm{SQL}} = 1/\sqrt{N}$ , that is,  $\xi^2 = (\Delta \phi/\Delta \phi_{\mathrm{SQL}})^2$ . The OAT dynamics can prepare spin squeezing where  $\xi^2$  ideally scales as  $N^{-2/3}$  (ref. 4). At longer evolution times, this model can also generate various

non-Gaussian states, such as q-headed cat states, whose metrological utility must be characterized through more complex, nonlinear quantities beyond the squeezing parameter, such as the quantum Fisher information<sup>30</sup>.

A similar model more accessible in a plethora of modern platforms<sup>31-34</sup> is the power-law Ising chain:

$$\hat{H}_{\text{PL-Ising}} = \frac{1}{2} \sum_{i < j} J_{i,j} \, \hat{\sigma}_i^z \hat{\sigma}_j^z, \tag{3}$$

in which  $J_{i,j} = J_0 | i-j |^{-\alpha}$  for exponent  $\alpha$ , resembling  $\hat{H}_{OAT}$  with the addition of a distance-dependent interaction. Its dynamics only approximate those of a collective OAT model, with  $\chi = \overline{J}$ , for sufficiently long-ranged interactions, in which  $\overline{J} = \sum_{i < j} J_{i,j} / (N(N-1)/2)$  is the average coupling between pairs of spins. For  $\alpha \ge D$ , this model ceases to exhibit scalable spin squeezing and only recovers the full  $N^{-2/3}$  scaling when  $\alpha < 2D/3$ , with D the dimensionality of the system<sup>35</sup>. This precludes  $\alpha = 1$  relevant for our D = 1 experiment.

Nonetheless, collective behaviour in the power-law Ising model may potentially be stabilized through the appropriate addition of Heisenberg-type interactions  $\hat{H}_{\text{PL-Heisenberg}} = \sum_{i < j} J_{i,j} \hat{\boldsymbol{o}}_i \cdot \hat{\boldsymbol{o}}_j / 2$ 

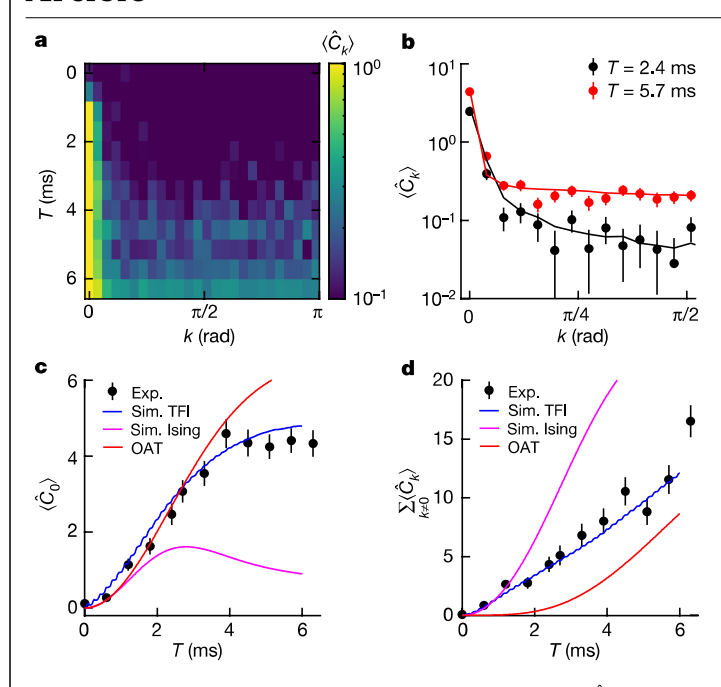


**Fig. 2** | **Structure factor. a**, Time evolution of the structure factor  $\langle \hat{C}_k \rangle$  with wavevector k in an N=51-ion chain with  $\alpha \approx 0.9$ . **b**, Measured structure factor components  $\langle \hat{C}_k \rangle$  at T=2.5 ms and 5.7 ms. Solid lines are numerical simulations for the TFI model. **c**, Time evolution of the k=0 correlation in comparison with simulated TFI, Ising and OAT models. **d**, Sum of the components with  $k \neq 0$ .

(refs. 25,27–29,36). A key example of this is the power-law XY model  $\hat{H}_{PL-XY} = \hat{H}_{PL-Heisenberg} - \hat{H}_{PL-Ising}$ , which results in distance-dependent exchange interactions of the form  $\hat{\boldsymbol{\sigma}}_{i} \cdot \hat{\boldsymbol{\sigma}}_{j} - \hat{\sigma}_{i}^{z} \hat{\sigma}_{j}^{z} = 2(\hat{\sigma}_{i}^{+}\hat{\sigma}_{j}^{-} + h.c.)$ .

In our trapped-ion quantum simulator of up to 51 ions, a pseudo-spin is encoded in two electronic states of  $^{40}$ Ca\*-the  $|\downarrow\rangle=|S_{1/2},m=+1/2\rangle$  and  $|\uparrow\rangle=|D_{5/2},m=+5/2\rangle$  states—which are collectively coupled by a global laser beam<sup>37</sup>. Spin—spin interactions between the ions are engineered by means of a two-tone laser that couples the internal electronic states of the ions to their ground-state-cooled transverse motional modes (see Methods sections 'Experimental platform' and 'Generation of spin—spin interaction'). With the application of a strong drive transverse to the interaction axis, the dynamics are described by the power-law transverse-field Ising (TFI) model,  $\hat{H}_{\text{PL-TFI}} = \sum_{i < j} \hat{J}_{ij} \hat{\sigma}_{i}^{x} \hat{\sigma}_{j}^{x} + B \sum_{i} \hat{\sigma}_{i}^{z}$ . By considering this system in the rotating frame of the drive, we can approximately describe it using the power-law XY model

$$\hat{H}_{\text{PL-XY}} = \sum_{i < j} J_{i,j} \left( \hat{\sigma}_i^{\dagger} \hat{\sigma}_j^{-} + \hat{\sigma}_i^{-} \hat{\sigma}_j^{\dagger} \right) \tag{4}$$

as previously reported, in which  $J_{i,j} = J_0 |i-j|^{-\alpha}$  (see Fig. 1b) sets the strength of interactions between sites i and j. The interactions strength is parametrized in terms of the nearest-neighbour strength  $J_0$  and a tunable exponent  $0 < \alpha < 3$  describing the interaction range.

## **Generation of spin-squeezed states**

We use a similar protocol for preparing spin-squeezed states as for the OAT, as sketched in Fig. 1a: we first prepare a CSS polarized along +x and then evolve this state under the XY interaction in equation (4) for a variable time T. In the experiment, the interaction period is split by an echo pulse that cancels site-dependent Stark shifts along z and increases the coherence time of the system.

In Fig. 1c, we investigate the dynamics of the Wineland squeezing parameter for two system sizes and interaction ranges. We find

an optimal value of  $\xi^2 = -3.9 \pm 0.3$  dB with N = 12 and  $\alpha \approx 1$  and  $\xi^2 = -3.7 \pm 0.5$  dB with N = 51 and  $\alpha \approx 0.9$ , comparable with levels of noise reduction generated in previous trapped-ion studies using larger arrays<sup>24</sup>. Despite the increased particle number in the latter case, we do observe a slight decrease in the attainable spin squeezing for this system, in contrast to the expected improvement according to the ideal OAT model. We attribute this to collective dephasing noise from magnetic-field fluctuations and laser noise, at a rate we characterize independently and can be included in our theoretical calculations (see Methods sections 'Mitigation of global dephasing effects' and 'Numerical methods'). To verify that this is the mechanism responsible for the reduction in spin squeezing, we compare the dynamics to that of the OAT model with coupling  $\chi = J$ , also in the presence of this collective dephasing. For both system sizes, we observe a similar reduction in the spin squeezing and we find that the observed dynamics are within 1 dB of the corresponding OAT dynamics, confirming that our dynamics are well approximated by the fully collective model and that indeed any reduction in the expected metrological gain is not a result of the reduced interaction range of our power-law model or other local decoherence mechanisms in the experiment. Furthermore, we compare to analogous calculations of equation (4) with decoherence, finding excellent agreement with the observed dynamics using the assessed decoherence rate. Lingering deviations between the two are small and largely accounted for by considering the underlying model in the presence of the transverse field, validating both our approximate use of the XY model as well as the validity of the approximate numerical methods we use (see Methods section 'Numerical methods'). Note that an exact calculation of the dynamics of equation (4) or the TFI model, in the presence of decoherence, is intractable at present for the range of N we consider.

To further investigate the collective nature of our system, we examine the value of the total spin  $(\hat{\mathbf{S}}^2)$  at the time at which the spin squeezing is found to be optimal, for a range of system sizes; see Fig. 1d. This observable commutes with the global dephasing operator and is thus unaffected by it. We observe that total spin decays slightly for larger N, as the finite range of the interactions is better resolved over larger chains, but seems to plateau to a relatively large value; this is consistent with numerical calculations of both the TFI and XY models. Furthermore, when compared with the state prepared by the Ising model with the same interaction range (equation (3)), the observed dynamics in our XY model remain relatively collective, consistent with theoretical predictions  $^{25,27,29}$ .

## Structure factor

Systems exhibiting non-uniform interactions will develop non-collective correlations characterized by a non-zero structure factor at finite wavenumber  $k \neq 0$ . In particular, the structure factor can be used to estimate the mode occupation  $\langle \hat{n}_k \rangle$  of linear SWE at short timescales (see Methods section 'Structure factor and linear spin-waves'):

$$\begin{split} \langle \hat{C}_{k} \rangle &\equiv \frac{1}{4N} \sum_{i,j} \langle (\hat{\sigma}_{i}^{y} - i\hat{\sigma}_{i}^{z})(\hat{\sigma}_{j}^{y} + i\hat{\sigma}_{j}^{z}) \rangle \cos(k(r_{i} - r_{j})) \\ &\simeq \frac{\langle \hat{n}_{k} + \hat{n}_{-k} \rangle}{2}. \end{split} \tag{5}$$

Using site-resolved measurements, we investigate the dynamics of  $\langle \hat{C}_k \rangle$  as it evolves according to the Hamiltonian (equation (4)).

In Fig. 2a,b, we observe a substantial growth of the k=0 component, whereas the populations of components with  $k\neq 0$  attain a relatively small growth over time, with the most notable growth observed for small values of |k|.

In Fig. 2c,d, we plot the dynamics of both the k=0 component and the sum of the non-zero components of the structure factor. Examining the measured data as well as the simulated TFI model, we observe

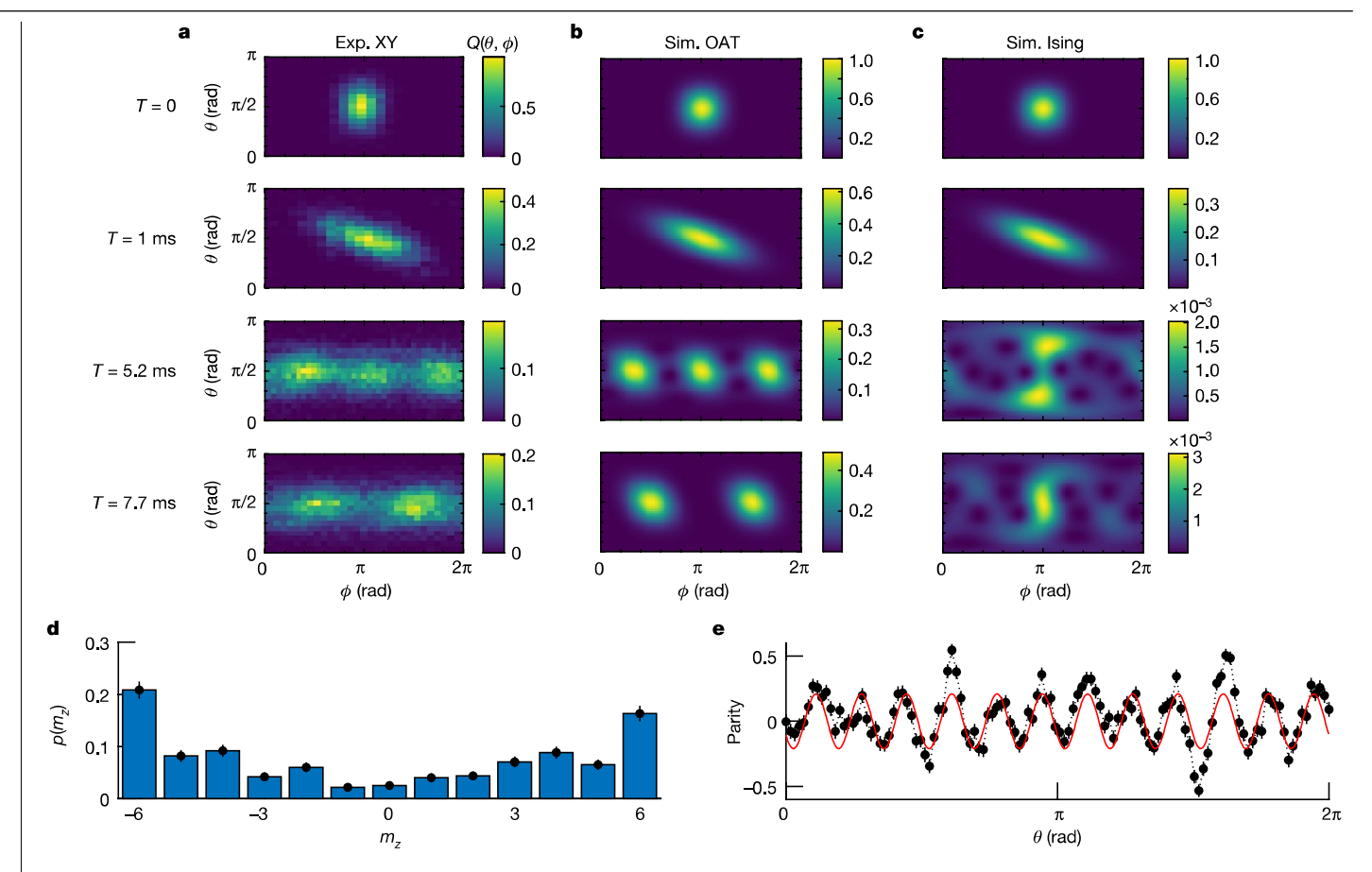


Fig. 3 | Husimi Q-distributions. a, Measured Husimi Q-distributions of 12-ion spin states for different interaction times T of the realized XY interaction with  $J_0 = 560 \,\mathrm{rad}\,\mathrm{s}^{-1}$ . Although the state evolves from a CSS to a SSS at short times, a three-headed cat state and a two-headed cat state are observed at later times. **b**,**c**, Simulated Husimi Q-distributions for an OAT model with  $\chi = \overline{J}$  and the power-law Ising model with the same interaction range as the experiment, at different interaction times T and without the effects of decoherence. For

 $illustrative\, reasons, the\, peaks\, of\, the\, distributions\, are\, centred\, by\, shifting\, the$ phase  $\phi$ . We adjust the colour scale of each plot to enhance the visibility of features of the phase-space distributions. d, Measured probabilities in all magnetization sectors  $m_x = (n_x - n_x)/2$  of the two-headed cat state. Here  $n_{x(x)}$  is the number of ions in the state  $|\uparrow\rangle(|\downarrow\rangle)$ . **e**, Parity oscillations of the two-headed cat state and corresponding sinusoidal fit in red to estimate the contrast  ${\it C}$ . The dotted black line is a guide to the eye.

a similar growth of the collective component and the non-collective components. However, in the corresponding power-law Ising model with the same interaction range, the population of the non-collective components quickly outpaces the growth of the collective components. This signifies a regime in which the dynamics are dominated by correlations with finite momenta and in which the linear spin-wave approximation breaks down.

Furthermore, the growth of the collective component initially resembles that of the corresponding OAT model, further validating the collective nature of our system. We note that, unlike spin squeezing, the structure factor is more resistant to global dephasing and we thus directly compare the observed experimental results with theoretical calculations of the OAT and power-law Ising models obtained by solving the ideal unitary dynamics.

## Q-functions: beyond the Gaussian regime

For evolution times beyond the optimal spin-squeezing time, the quantum noise distribution in the OAT model starts to develop various non-Gaussian states, a set of which are the family of q-headed cat states<sup>5-7,27</sup>. Of these states, the multi-headed cat state with q = 2state corresponds to the well-known Greenberger-Horne-Zeilinger state<sup>38</sup>.

To explore and characterize the survival of the collective non-Gaussian states in the dynamics under equation (4), we directly

measure the evolution of the Husimi Q-distribution  $Q(\theta, \phi)$  =  $\langle \mathbf{n}(\theta,\phi)|\hat{\rho}|\mathbf{n}(\theta,\phi)\rangle$ , in which  $\hat{\rho}$  is the density matrix of our state and  $|\mathbf{n}(\theta, \phi)\rangle$  is the CSS with polarization vector **n** characterized by polar/ azimuthal angles  $\theta/\phi$  on the collective Bloch sphere. In Fig. 3, we show the measured Q-distribution for various times in the evolution. Starting from the initial CSS at T = 0, we initially observe the development of a SSS at short times. At specific later times, we observe the fracturing of the Q-distribution into various distinct patches, with the distribution characterized by q such patches occurring at time  $T = \pi/q \overline{J}$ .

We plot theoretical calculations for the analogous OAT model (with  $\chi = \overline{I}$ ) in the absence of decoherence for comparison and observe that our measured phase-space structure correlates well with the evolution of this fully collective model. Relative to the OAT model, the measured patches are smeared out in the horizontal direction, as a result of collective dephasing, but this smearing remains small enough to resolve the underlying separation of the Q-distribution. We also show the analogous results for the power-law Ising model in the absence of decoherence and with the same interaction range. Its quantum noise distribution beyond the Gaussian regime shows little resemblance in shape and magnitude to the OAT model (note very different scale in Fig. 3c).

To explore the presence of coherence between each of the observed coherent spin-like states, we measure parity oscillations for the q = 2cat state with contrast C, which, in combination with the projection of our state onto the  $\pm N/2$  eigenstates of  $\hat{S}_{z}$  and the corresponding probabilities  $p(m_z = \pm N/2)$  (see Fig. 3d,e), yields a measure of fidelity to the

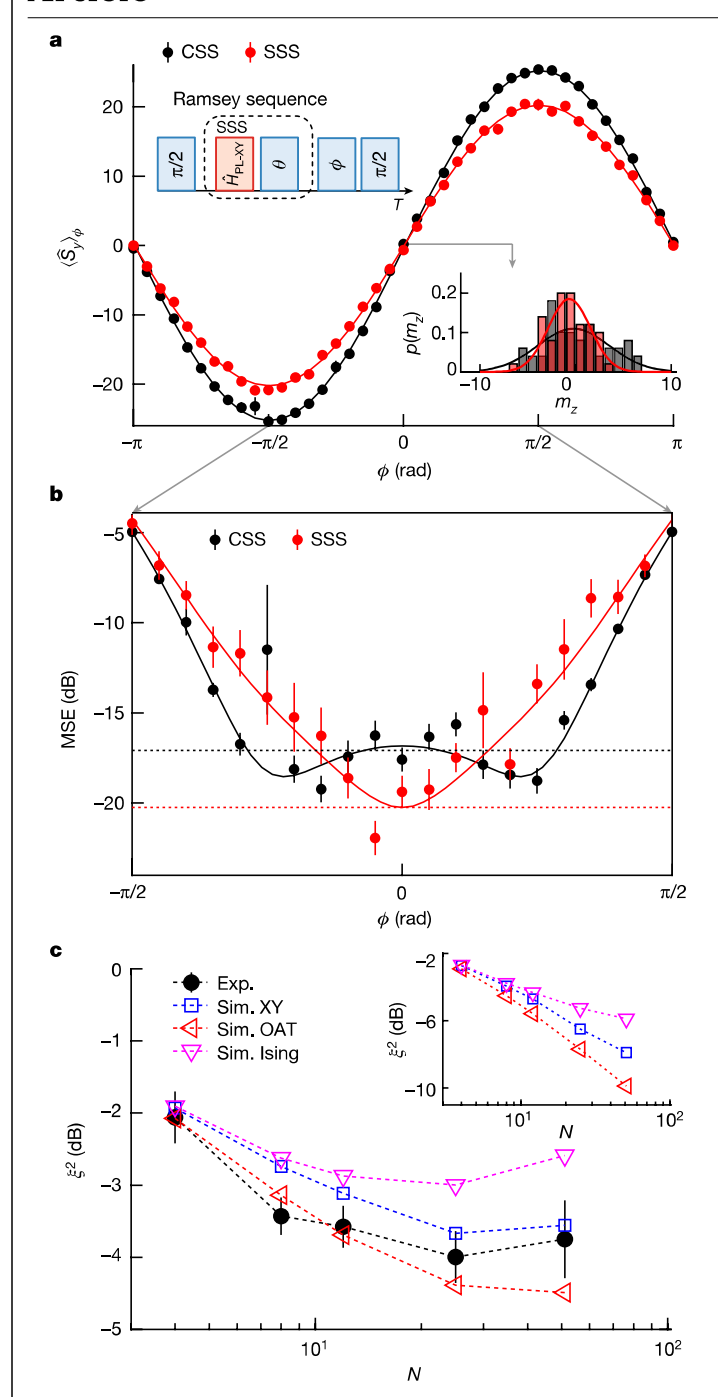


Fig. 4 | Phase estimation with a CSS and a SSS of 51 qubits. a, Experimentally measured Ramsey fringe  $\langle \hat{S}_{\nu} \rangle_{\phi}$  (see Methods section 'Measurements') as a function of the phase  $\phi$  imprinted onto the ions. Insets, Ramsey pulse sequence including the preparation and alignment by some angle  $\theta$  of the SSS and probability to obtain the measurement outcomes  $m_z$  after the Ramsey sequence for  $\phi = 0$ . **b**. MSE between imprinted and estimated phases as a function of  $\phi$  (see equation (9)). The dashed black line indicates the standard quantum limit 1/N and the dashed red line indicates the gain in sensitivity of 3.2 dB for the SSS over the standard quantum limit. Solid lines are fits to the respective models (see Methods section 'Measurements').  ${\bf c}$ , Dependence of  $\xi^2$ on the system size. The error bars are obtained through the jackknife resampling method. We show comparisons with simulations for the power-law XY model, for the OAT model with  $\chi = \overline{J}$  and for the power-law Ising model, all with effects of global dephasing taken into account (the dashed lines are guides to the eye). The inset shows simulations of the respective models without decoherence.

ideally prepared q=2 cat state  $F=[p(m_z=N/2)+p(m_z=-N/2)+C]/2$ . We observe the clear presence of parity oscillations in Fig. 3e. The generated state has a fidelity of  $F=0.28\pm0.02$ , which is below the required 0.5 to certify N-partite entanglement. We attribute this relative lack of fidelity primarily to decoherence in this system. Exact theoretical calculations in the absence of decoherence predict that fidelities of up to 0.916 can be achieved for the 12-ion XY model with  $\alpha\approx1$  (the fidelity decreases to 0.865 if the finite transverse field is taken into account). On the contrary, a decoherence-free Ising model with the same interaction range results in a fidelity of <0.002 at  $T=\pi/2\bar{J}$ .

## Phase sensing with a 51-ion chain

To study the performance of a SSS in a Ramsey interferometer, we first prepare a SSS with our finite-range interaction and thereafter align the minimum variance axis of the variance ellipse perpendicular to the measurement axis (z-axis) by performing a rotation operation as described in Methods section 'Measurements'. The phase  $\phi$  is then imprinted on the spin vector by performing a rotation about the Bloch sphere z-axis. The projection of the spin along the y-axis shows sinusoidal variation of  $\langle \hat{S}_y \rangle_{\phi}$ , with  $\hat{S}_y = \frac{1}{2} \sum_j \hat{\sigma}_j^y$ , as a function of imprinted phases for both CSS and SSS cases, as shown in Fig. 4a. In the inset, we show the measured histogram of  $m_{z^z}$  eigenvalues of the  $\hat{S}_z$ , from the single-shot outcomes in the measurement axis and demonstrate the narrowing of the distribution when a spin-squeezed state is used.

In practice, the measurement outcome of  $m_z$  is used to estimate the imprinted phase  $\phi$ . We use a linear estimator to find the imprinted phases on collective spin and calculate the mean squared error (MSE) for the SSS and the CSS. The results are presented in Fig. 4b. Notably, a reduction in the MSE is visible when the SSS is used over the CSS for small values of  $\phi$  around  $\phi=0$ . For large values of  $\phi$ , the estimator performs poorly for both cases owing to the fact that our estimator is only unbiased for  $\phi=0$ .

In Fig. 4c, we show a scaling of the achievable spin squeezing as a function of the system size N, maintaining a fixed  $J_0$ . The experimental results indicate an increase in  $\xi^2$  for small N but for large N saturation occurs. The inset shows the ideal scaling of the three models, without decoherence. In our system, the current limitation is imposed by slow entanglement generation and underlying dephasing channels, as we again confirm that the optimal squeezing is similar to that achievable in an analogous OAT model with  $\chi=J$  and decoherence and dephasing taken into account. One could improve this by either increasing the spin–spin coupling strength or by reducing the dephasing effects. In fact, we already observe an improvement when the value of  $J_0$  is doubled, while maintaining the same level of dephasing (see N=12 in Fig. 1c).

## Conclusion

The direct observation of emergent collective dynamical behaviours, similar to what is achievable with OAT, in a system with finite-range interactions represents a crucial step towards integrating entanglement into clocks that operate with a substantial number of particles. Although we have demonstrated the use of spin-exchange interactions to preserve spin alignment in a 1D chain, far better protection is expected to be achieved in optical qubits trapped in higher spatial dimensions<sup>25-29</sup>, such as planar Coulomb crystals built using new monolithic radiofrequency traps<sup>39,40</sup>, or Penning traps<sup>24,41</sup>, as well as in optical tweezer arrays <sup>22,42–44</sup> and 3D optical lattices <sup>45</sup>. Furthermore, although squeezed states generated by OAT do not saturate the 1/N Heisenberg limit in standard Ramsey protocols, the corresponding interactions can be combined with time-reversal-based schemes<sup>46</sup> or series of global rotations<sup>47</sup> to achieve a Heisenberg scaling. Moreover, the emergent collective dynamics of the XY model can be used to enrich the gate toolset for programmable quantum sensors<sup>48,49</sup> and enhance their capability

to measure time-varying frequencies close to the fundamental limit imposed by quantum mechanics in larger arrays.

During completion of our work, we became aware of related experiments using dressed Rydberg interactions in tweezer<sup>43,44</sup> and microtrap<sup>50</sup> array platforms.

## **Online content**

Any methods, additional references, Nature Portfolio reporting summaries, source data, extended data, supplementary information, acknowledgements, peer review information; details of author contributions and competing interests; and statements of data and code availability are available at https://doi.org/10.1038/s41586-023-06472-z.

- Bothwell, T. et al. Resolving the gravitational redshift across a millimetre-scale atomic sample, Nature 602, 420-424 (2022).
- Oelker, E. et al. Demonstration of  $4.8 \times 10^{-17}$  stability at 1 s for two independent optical clocks. Nat. Photon. 13, 714-719 (2019).
- McGrew, W. F. et al. Atomic clock performance enabling geodesy below the centimetre level. Nature 564, 87-90 (2018).
- Kitagawa, M. & Ueda, M. Squeezed spin states. Phys. Rev. A 47, 5138 (1993).
- Agarwal, G., Puri, R. & Singh, R. Atomic Schrödinger cat states. Phys. Rev. A 56, 2249
- 6. Mølmer, K. & Sørensen, A. Multiparticle entanglement of hot trapped ions. Phys. Rev. Lett. 82. 1835 (1999).
- Song, C. et al. Generation of multicomponent atomic Schrödinger cat states of up to 20 aubits. Science 365, 574-577 (2019).
- Comparin, T., Mezzacapo, F. & Roscilde, T. Multipartite entangled states in dipolar quantum simulators. Phys. Rev. Lett. 129, 150503 (2022).
- Wineland, D. J., Bollinger, J. J., Itano, W. M., Moore, F. L. & Heinzen, D. J. Spin squeezing and reduced quantum noise in spectroscopy. Phys. Rev, A 46, R6797 (1992).
- Wineland, D. J., Bollinger, J. J., Itano, W. M. & Heinzen, D. J. Squeezed atomic states and projection noise in spectroscopy. Phys. Rev. A 50, 67 (1994).
- Giovannetti, V., Lloyd, S. & Maccone, L. Advances in quantum metrology. Nat. Photon. 5,
- Degen, C. L., Reinhard, F. & Cappellaro, P. Quantum sensing. Rev. Mod. Phys. 89, 035002
- Pezzè, L., Smerzi, A., Oberthaler, M. K., Schmied, R. & Treutlein, P. Quantum metrology
- with nonclassical states of atomic ensembles. Rev. Mod. Phys. 90, 035005 (2018). Ludlow, A. D., Boyd, M. M., Ye, J., Peik, E. & Schmidt, P. O. Optical atomic clocks. Rev. Mod. Phys. 87, 637 (2015).
- Norcia, M. A. et al. Cavity-mediated collective spin-exchange interactions in a strontium superradiant laser. Science 361, 259-262 (2018).
- Ritsch, H., Domokos, P., Brennecke, F. & Esslinger, T. Cold atoms in cavity-generated dynamical optical potentials. Rev. Mod. Phys. 85, 553 (2013).
- Leroux, I. D., Schleier-Smith, M. H. & Vuletić, V. Implementation of cavity squeezing of a collective atomic spin. Phys. Rev. Lett. 104, 073602 (2010).
- Hosten, O., Engelsen, N. J., Krishnakumar, R. & Kasevich, M. A. Measurement noise 100 times lower than the quantum-projection limit using entangled atoms. Nature 529, 505-508 (2016).
- Cox, K. C., Greve, G. P., Weiner, J. M. & Thompson, J. K. Deterministic squeezed states with collective measurements and feedback. Phys. Rev. Lett. 116, 093602 (2016).
- Pedrozo-Peñafiel, E. et al. Entanglement on an optical atomic-clock transition. Nature 588, 414-418 (2020).
- Bohn, J. L., Rey, A. M. & Ye, J. Cold molecules: progress in quantum engineering of chemistry and quantum matter. Science 357, 1002-1010 (2017).
- Schine, N., Young, A. W., Eckner, W. J., Martin, M. J. & Kaufman, A. M. Long-lived Bell states in an array of optical clock qubits. Nat. Phys. 18, 1067-1073 (2022).
- Britton, J. W. et al. Engineered two-dimensional Ising interactions in a trapped-ion quantum simulator with hundreds of spins. Nature 484, 489-492 (2012).

- Bohnet, J. G. et al. Quantum spin dynamics and entanglement generation with hundreds of trapped ions. Science 352, 1297-1301 (2016).
- Perlin, M. A., Qu, C. & Rey, A. M. Spin squeezing with short-range spin-exchange interactions. Phys. Rev. Lett. 125, 223401 (2020).
- Bilitewski, T. et al. Dynamical generation of spin squeezing in ultracold dipolar molecules. Phys. Rev. Lett. 126, 113401 (2021).
- Comparin, T., Mezzacapo, F. & Roscilde, T. Robust spin squeezing from the tower of states of U(1)-symmetric spin Hamiltonians. Phys. Rev. A 105, 022625 (2022).
- Young, J. T., Muleady, S. R., Perlin, M. A., Kaufman, A. M. & Rey, A. M. Enhancing spin squeezing using soft-core interactions. Phys. Rev. Res. 5, L012033 (2023).
- Block, M. et al. A universal theory of spin squeezing. Preprint at https://arxiv.org/ abs/2301.09636 (2023).
- Pezzé, L. & Smerzi, A. Entanglement, nonlinear dynamics, and the Heisenberg limit. Phys. Rev. Lett. 102, 100401 (2009).
- Browaeys, A. & Lahaye, T. Many-body physics with individually controlled Rydberg atoms. Nat. Phys. 16, 132-142 (2020).
- Bruzewicz, C. D., Chiaverini, J., McConnell, R. & Sage, J. M. Trapped-ion quantum computing: progress and challenges. Appl. Phys. Rev. 6, 021314 (2019)
- Tscherbul, T. V., Ye, J. & Rey, A. M. Robust nuclear spin entanglement via dipolar interactions in polar molecules. Phys. Rev. Lett. 130, 143002 (2023).
- Gorshkov, A. V. et al. Tunable superfluidity and quantum magnetism with ultracold polar molecules. Phys. Rev. Lett. 107, 115301 (2011).
- Foss-Feig, M., Gong, Z.-X., Gorshkov, A. V., and Clark, C. W. Entanglement and spin-squeezing without infinite-range interactions. Preprint at https://arxiv.org/abs/ 1612.07805 (2016).
- Rey, A. M., Jiang, L., Fleischhauer, M., Demler, E. & Lukin, M. D. Many-body protected entanglement generation in interacting spin systems. Phys. Rev. A 77, 052305 (2008).
- Kranzl, F. et al. Controlling long ion strings for quantum simulation and precision measurements. Phys. Rev. A 105, 052426 (2022).
- Greenberger, D. M., Horne, M. A. & Zeilinger, A. in Bell's Theorem, Quantum Theory and Conceptions of the Universe (ed. Kafatos, M.) 69-72 (Springer, 1989).
- Qiao, M. et al. Observing frustrated quantum magnetism in two-dimensional ion crystals. Preprint at https://arxiv.org/abs/2204.07283 (2022).
- Kiesenhofer, D. et al. Controlling two-dimensional Coulomb crystals of more than 100 ions in a monolithic radio-frequency trap. PRX Quantum 4, 020317 (2023).
- Itano, W. M. et al. Bragg diffraction from crystallized ion plasmas. Science 279, 686-689
- 42. Barredo, D., Lienhard, V., de Léséleuc, S., Lahaye, T. & Browaeys, A. Synthetic threedimensional atomic structures assembled atom by atom. Nature 561, 79-82 (2018).
- Bornet, G. et al. Scalable spin squeezing in a dipolar Rydberg atom array. Preprint at https://arxiv.org/abs/2303.08053 (2023)
- Eckner, W. J. et al. Realizing spin squeezing with Rydberg interactions in a programmable optical clock. Preprint at https://arxiv.org/abs/2303.08078 (2023)
- Campbell, S. L. et al. A Fermi-degenerate three-dimensional optical lattice clock. Science 358, 90-94 (2017).
- 46. Davis, E., Bentsen, G. & Schleier-Smith, M. Approaching the Heisenberg limit without single-particle detection. Phys. Rev. Lett. 116, 053601 (2016).
- Liu, Y. C., Xu, Z. F., Jin, G. R. & You, L. Spin squeezing: transforming one-axis twisting into two-axis twisting. Phys. Rev. Lett. 107, 013601 (2011).
- 48. Marciniak, C. D. et al. Optimal metrology with programmable quantum sensors. Nature 603, 604-609 (2022).
- Kaubruegger, R., Vasilyev, D. V., Schulte, M., Hammerer, K. & Zoller, P. Quantum variational optimization of Ramsey interferometry and atomic clocks. Phys. Rev. X 11, 041045 (2021).
- Hines, J. A. et al. Spin squeezing by Rydberg dressing in an array of atomic ensembles. Preprint at https://arxiv.org/abs/2303.08805 (2023).

**Publisher's note** Springer Nature remains neutral with regard to jurisdictional claims in published maps and institutional affiliations.

Springer Nature or its licensor (e.g. a society or other partner) holds exclusive rights to this article under a publishing agreement with the author(s) or other rightsholder(s); author self-archiving of the accepted manuscript version of this article is solely governed by the terms of such publishing agreement and applicable law.

© The Author(s), under exclusive licence to Springer Nature Limited 2023

## Methods

## **Experimental platform**

The experiment is performed on an analogue quantum simulator based on trapped ions held in a macroscopic linear Paul trap<sup>37</sup>. Two electronic states, namely  $S_{1/2}$ , m = +1/2 and  $D_{5/2}$ , m = +5/2, of a trapped <sup>40</sup>Ca<sup>+</sup> ion form two pseudo-spin states  $|\downarrow\rangle$  and  $|\uparrow\rangle$ , respectively.

Long ion chains are held in the trap by a confining force in the radial directions, generated by a 2D rf-quadrupole field that creates centre-of-mass (COM) mode frequencies of about 2.93 MHz and 2.89 MHz. A set of dc voltages provides a weakly confining force along the direction of the rf-quadrupole and controls the frequency splitting of the transverse COM modes. The axial trapping potentials are tuned in such a way as to achieve COM mode frequencies between  $\omega_z = 2\pi \times 117$  kHz and  $\omega_z = 2\pi \times 479$  kHz for ion numbers between 51 and 4. Before initializing the ions into the desired spin states, the transverse motional modes of the ion chain are cooled close to the motional ground state by means of Doppler cooling and resolved sideband cooling techniques. Axial modes are sub-Doppler-cooled using the polarization gradient cooling technique.

A frequency-stable laser with a linewidth below 10 Hz and a wavelength of about 729 nm is used for coherent qubit manipulation by globally illuminating all ions from the radial direction with an elliptically shaped laser beam with a near spatial homogeneity. All ions are dissipatively initialized in the spin-down state. Thereafter, the collective spin vector is prepared along the *x*-axis by applying a global laser pulse that rotates the spin vector about the –*y*-axis. A composite pulse sequence is implemented to reduce the effects of the spatial inhomogeneity of the laser beam. More details can be found in the supplemental materials of ref. 51.

## Generation of spin-spin interaction

The ions are entangled by means of a two-tone laser field driving the spin and the radial motional degrees of freedom<sup>52</sup>. The unwanted Stark shift generated from the coupling of the laser field to other electronic states is compensated by adding a third laser frequency component onto the two-tone field. This resultant field generates a global spin-spin interaction between the ions, representing a power-law-decaying Ising-type interaction. In our experiments, the two-tone laser field is detuned by a frequency between 48 kHz and 25 kHz, for ion numbers between 4 and 51, from the highest frequency mode. The third laser beam is detuned by +1.4 MHz from the carrier transition. The centre frequency of the two-tone field is detuned from the spin resonance to engineer a TFI interaction,

$$\hat{H}_{\text{PL-TFI}} = \sum_{i < j} \frac{J_0}{|i - j|^{\alpha}} \hat{\sigma}_i^x \hat{\sigma}_j^x + B \sum_i \hat{\sigma}_i^z.$$
 (6)

The transverse components trength is  $B = 9,500 \, \text{rad s}^{-1}$  and  $J_0 \le 560 \, \text{rad s}^{-1}$ , thus allowing us to transform the above interaction into the XY interaction in the frame rotating with the transverse field, by neglecting the resulting fast oscillating terms (rotating-wave approximation).

## Mitigation of global dephasing effects

The fluctuation of laser phase and ambient magnetic fields incur dephasing of the spins during the preparation of the spin-squeezed state. The magnetic-field fluctuations are predominately caused by the current flowing in the electrical appliances in the laboratory thus having contribution at 50 Hz and its higher-order harmonics. Further details of mitigating these magnetic-field fluctuations through a feedforward method are presented in ref. 37. The remaining dephasing induced by the slow phase variation of the laser field and the transition frequency change is reduced in our case by the spin-echo technique and we observe an improvement in  $T_2$  coherence time from  $42 \pm 2$  ms to  $68 \pm 6$  ms after implementing the spin-echo scheme.

For fast-varying components not eliminated by the spin echo, we model this as collective white-noise dephasing in our numerical simulations presented in the text (see also Methods section 'Numerical methods'). Modelling this with a dephasing rate determined by the  $T_2$  coherence time in the presence of a spin-echo, we find a good agreement between experimental and simulation results without the use of any free parameters. This suggests that collective dephasing is the limiting noise factor in our system.

Moreover, other noise sources, such as unwanted coupling to motional sidebands, that lead to a change of magnetization in the otherwise magnetization-conserving interaction are characterized independently. The measured rate of these noise sources is  $1\,\mathrm{s}^{-1}$  per ion, which is an order of magnitude smaller than the collective dephasing rates.

#### Measurements

To evaluate the various quantities presented in this manuscript, we perform a collective rotation of the spins

$$\hat{R}(\tilde{\theta}, \tilde{\phi}) = \prod_{j} e^{-i\frac{\tilde{\theta}}{2}(\hat{\sigma}_{j}^{x}\cos\tilde{\phi} + \hat{\sigma}_{j}^{y}\sin\tilde{\phi})}, \tag{7}$$

as sketched in Extended Data Fig. 1a. The spins are rotated by an angle  $\widetilde{\theta}$  around an arbitrary axis in the xy-plane that is parametrized by  $\widetilde{\phi}$ . Followed by a projective measurement in the z-basis, this allows us to measure the collective spin operators in any basis  $\hat{S}_{\theta,\phi} = \hat{R}^{\dagger}(\widetilde{\theta},\widetilde{\phi})$   $\hat{S}_z$   $\hat{R}(\widetilde{\theta},\widetilde{\phi})$  characterized by polar/azimuthal angles  $\theta/\phi$  on the collective Bloch sphere. Here the polar/azimuthal angles are related to rotation angles by  $\phi = \widetilde{\phi} + \pi/2$  and  $\theta = \widetilde{\theta}$ .

Spin-squeezing parameter. To estimate the spin-squeezing parameter (equation (2)), we perform a set of measurements in which either  $\phi$  or  $\theta$  are scanned. The evolution under the TFI model changes the orientation of the collective spin vector in contrast to the XY model, thus consecutive laser pulses are needed to be operated under the knowledge of this phase accumulation. In our experiments, the transverse field is engineered by detuning the laser field by the strength  $B \gg J_0$  such that the rotating-wave approximation is met, whereas the spin-vector rotation is accounted for by the phase evolution of the detuned laser field during the operation of TFI interaction. Nonetheless, we still observe small changes in the spin orientation within the xy-plane, which can arise owing to changes in the transition frequency from unaccounted factors. To characterize the length of the spin vector and its orientation, we perform a set of measurements  $\langle \hat{S}_{\pi/2,\phi} \rangle$  in which the measurement basis is changed within the xy-plane. These quantities are estimated by fitting the experimental data (see Extended Data Fig. 1b for two representative fits) by a sin function. The length of the spin vector is given by the contrast of the fit and phase offset  $\phi_0$  represents the angle between the spin vector and the

In a subsequent series of measurements, we measure  $\langle (\Delta \hat{S}_{\theta,\phi_0})^2 \rangle$  for different  $\theta$ , which corresponds to a scan of the variance in the plane orthogonal to the mean spin direction. To determine the minimal orthogonal variance and the angle at which this variance is aligned with the z-axis, we fit  $\langle (\Delta \hat{S}_{\theta,\phi_0})^2 \rangle$  by a fit function of the form  $V(\theta) = (V_{\text{max}} - V_{\text{min}}) \sin^2(\theta - \theta_0) + V_{\text{min}} (\text{see Extended Data Fig. 1c for two representative fits), such that <math>V_{\text{min}} = 4 \langle (\Delta \hat{S}_{\textbf{n}})^2 \rangle$ .

The same sets of measurements can be used to evaluate the correlation functions in the three Cartesian bases underlying the results presented in Figs. 1d and 2. Correlations in the x(y)-basis are evaluated from the dataset with  $\widetilde{\theta} = \pi/2$  for  $\widetilde{\phi} = 3\pi/2(0)$  and correlations in the z-basis are evaluated from the second set with  $\widetilde{\phi} = \phi_0$  at  $\theta = 0$ .

**Husimi Q-distribution.** The Husimi  $Q(\theta, \phi)$ -distributions visualized in Fig. 3 are obtained by measuring the overlap between the state  $|\psi\rangle$  after

the final rotation  $\hat{R}(\hat{\theta}, \widetilde{\phi})$  and the maximally polarized state  $|\downarrow, ..., \downarrow\rangle$ , such that

$$Q(\theta, \phi) = |\langle \psi, ..., \psi | \hat{R}(\widetilde{\theta}, \widetilde{\phi}) | \psi \rangle|^2, \tag{8}$$

which is equivalent to measuring the overlap with a coherent spin state  $|\mathbf{n}(\theta, \phi)\rangle = \hat{R}^{\dagger}(\widetilde{\theta}, \widetilde{\phi})|\downarrow, ..., \downarrow\rangle$ .

Characterization of the two-headed cat state. To characterize the two-headed cat state in Fig. 3d,e, we first rotate the cat state with a pulse  $\hat{R}(\pi/2,\phi_1)$ , in which  $\phi_1$  is chosen such that the axis of the cat state is aligned with the z-axis, that is, the Husimi distribution of the aligned state is maximal at the north and south poles. The probability distribution  $p(m_z) = |\langle m_z| \text{cat} \rangle|^2$  in Fig. 3d is obtained by projecting the aligned cat state onto the magnetization eigenstates  $\hat{S}_z \mid m_z \rangle = m_z \mid m_z \rangle$ . To evaluate the parity oscillation in Fig. 3e, we perform another rotation pulse  $\hat{R}(\pi/2,\widetilde{\phi})$  and measure the parity according to  $\langle \hat{P}_{\phi} \rangle = \sum_{m_z} \mathrm{e}^{-\mathrm{i}\pi(S+m_z)} |\langle m_z | \hat{R}(\pi/2,\widetilde{\phi}) | \text{cat} \rangle|^2$ . The phase factor  $\mathrm{e}^{-\mathrm{i}\pi(S+m_z)}$  is +1 (-1) if the number of ions in the excited state is even (odd).

**Phase-sensing experiment.** In Fig. 4, we study the metrological utility of the SSS we have prepared in terms of a Ramsey experiment. To perform a Ramsey experiment, the minimum variance direction of the SSS has to be aligned with the *y*-axis before the phase  $\phi$  to be sensed is imprinted according to a unitary  $\hat{U}(\phi) = \mathrm{e}^{-\mathrm{i}\phi\hat{S}_z}$  before the last step of a  $\pi/2$  pulse around the *x*-axis is applied and the ions are projectively measured. We can combine phase imprinting  $\hat{R}_z = \mathrm{e}^{-\mathrm{i}S_z\phi}$  and the final measurement pulse  $\hat{R}(\pi/2, 0)$  in a single rotation such that the Ramsey fringes are given by  $\langle \hat{S}_y \rangle_{\phi} = -\langle \hat{R}^{\dagger}(\pi/2, \phi) \hat{S}_z \hat{R}(\pi/2, \phi) \rangle$ .

fringes are given by  $\langle \hat{S}_y \rangle_{\phi} = -\langle \hat{R}^{\dagger}(\pi/2, \phi) \hat{S}_z \hat{R}(\pi/2, \phi) \rangle$ . To study the sensitivity of our spin-squeezed sensor, we consider an estimator  $\phi_{\rm est}(m) = m/|\langle \hat{\mathbf{S}} \rangle|$  that estimates the phase based on a single measurement of the magnetization m. We extract  $|\langle \hat{\mathbf{S}} \rangle|$  from the Ramsey fringe. For this estimator, the MSE can be expressed in terms of measurable expectation values according to

$$MSE(\phi) = \sum_{m=-N/2}^{N/2} (\phi - \phi_{est}(m))^2 p(m|\phi)$$

$$= \phi^2 - \frac{2\phi \langle \hat{S}_y \rangle_{\phi}}{|\langle \hat{\mathbf{S}} \rangle|^2} + \frac{\langle (\hat{S}_y)^2 \rangle_{\phi}}{|\langle \hat{\mathbf{S}} \rangle|^2}$$
(9)

Here the conditional probability is given by  $p(m|\phi) = |\langle m|\hat{S}_y|\psi_\phi\rangle|^2$ . The experimental data in Fig. 4b are fitted to a function MSE( $\phi$ ) =  $(\phi^2 + a_1\phi\sin\phi + a_2\sin^2\phi + a_3\cos^2\phi)$  after generalizing equation (9). We use the fit parameter  $a_3$  to determine the smallest MSE at  $\phi$  = 0 to be  $10\log_{10}(a_3)$  for a CSS and a SSS, respectively.

#### Error estimation in the measurements

In this work, each measurement point is an average of 50 to 600 repetitions of experimental realizations. Measurement error bars in this manuscript are produced using the jackknife resampling method<sup>53</sup>. Errors for numbers that are estimated from measurements in several bases are estimated with the error-propagation formula.

#### **Numerical methods**

For calculations involving evolution under the OAT model, we can exactly solve the wave equation for virtually any N, taking advantage of the permutation symmetry in this model. For the power-law Ising model, we can likewise solve for the full, exact dynamics for small N, whereas exact analytical results are available for the dynamics of arbitrary one-body and two-body observables<sup>54</sup>.

To include the effects of a white-noise global dephasing process in the dynamics, we use the master equation formalism to model the dynamics of density operator  $\hat{\rho}(T)$  of the state as

$$\partial \widehat{\rho}(T)/\partial T = -i[\widehat{H},\widehat{\rho}(T)] + \Gamma_z \left(\widehat{S}_z \widehat{\rho}(T)\widehat{S}_z - \frac{1}{2} \{\widehat{S}_z^2,\widehat{\rho}(T)\}\right)$$
(10)

for any of the Hamiltonians  $\hat{H}$  we model in the main text, in which we assume that the global dephasing rate is given by  $\Gamma_z = 2/T_2$ . To solve for the corresponding dynamics, we note that the jump operator  $\hat{S}_z$  commutes with the OAT Hamiltonian, as well as the power-law Ising and XY Hamiltonians, and thus we can directly compute its effects on the resulting observables and correlators after solving for the unitary dynamics. This can be performed exactly by the following replacements:

$$\langle \hat{S}_{x/y}(T) \rangle \rightarrow e^{-\Gamma_z T/2} \langle \hat{S}_{x/y}(T) \rangle$$
 (11)

$$\langle \hat{S}_{x/y} \hat{S}_z(T) \rangle \rightarrow e^{-\Gamma_z T/2} \langle \hat{S}_{x/y} \hat{S}_z(T) \rangle$$
 (12)

$$\langle (\hat{S}_x^2 - \hat{S}_y^2)(T) \rangle \rightarrow e^{-2\Gamma_z T} \langle (\hat{S}_x^2 - \hat{S}_y^2)(T) \rangle$$
 (13)

$$\langle \{\hat{S}_x, \hat{S}_y\}(T)\rangle \to e^{-2\Gamma_z T} \langle \{\hat{S}_x, \hat{S}_y\}(T)\rangle, \tag{14}$$

for the anticommutator  $\{\cdot,\cdot\}$ , in which  $\Gamma_z$  is the rate of global dephasing. For modelling the dynamics of the TFI model in equation (6), as well as the corresponding XY model in the large transverse-field limit, we must resort to more efficient, approximate schemes for larger N. Furthermore, we must explicitly solve for the effects of the global dephasing in the dynamics for the TFI model, as the corresponding jump operator no longer commutes with the Hamiltonian dynamics. To do this, we use the dissipative discrete truncated Wigner approximation (DDTWA) $^{55-57}$  to efficiently solve for the quantum dynamics when N > 10 for these two models (otherwise, we resort to exact methods). DDTWA has previously been benchmarked for calculations of quantum spin dynamics and spin-squeezing generation for various models $^{28,58}$  and affords an efficient semiclassical description of the dynamics.

To do this, we introduce classical variables  $S_i^{\mu}$  corresponding to the value of  $\langle \hat{\sigma}_i^{\mu} \rangle$ . For an initial spin-polarized state along +x, for example, we form a discrete probability distribution (Wigner function)

$$W(S_i) = \frac{1}{4} \delta(S_i^x - 1) \left[ \delta(S_i^y - 1) + \delta(S_i^y + 1) \right] \times \left[ \delta(S_i^z - 1) + \delta(S_i^z + 1) \right].$$
(15)

This corresponds to the four phase-space points  $(S_i^x, S_i^y, S_i^z) = (1, 1, 1), (1, 1, -1), (1, -1, 1), (1, -1, -1)$ , each occurring with equal probability 1/4 for each spin. We can then solve the coherent dynamics by evolving these variables using the corresponding mean-field equations for the relevant Hamiltonian, combined with randomly sampling initial values for  $(S_i^x, S_i^y, S_i^z)_{1 \le i \le N}$  according to the above distribution, independently for each i. For an ensemble of such trajectories, quantum expectation values may then be approximated by  $\langle \hat{\sigma}_i^\mu(t) \rangle \approx \overline{S_i^\mu(t)}$ , in which the overbar denotes averaging over all trajectories. We can also compute symmetrically ordered correlators using  $\langle (\hat{\sigma}_i^\mu \hat{\sigma}_j^\nu + \hat{\sigma}_j^\nu \hat{\sigma}_i^\mu)(t) \rangle / 2 \approx \overline{S_i^\mu(t)} S_j^\nu(t)$ . This averaging can lead to effects beyond mean-field theory arising from the underlying quantum noise distribution, owing to the generic nonlinear nature of the mean-field equations for an interacting system.

To model the effects of the global dephasing, we can include a stochastic contribution to our mean-field equations; see refs. 28,57. For example, for evolution under the XY interaction in equation (4), the resulting equations of motion for our classical variables are then given by the set of Stratonovich stochastic differential equations

$$dS_i^x = -\sum_{j \neq i} J_{i,j} S_i^z S_j^y dT - \sqrt{\Gamma_z} S_i^y dW^z$$
 (16)

$$dS_i^y = \sum_{i \neq i} J_{i,j} S_i^z S_j^x dT + \sqrt{\Gamma_z} S_i^x dW^z$$
(17)

$$dS_i^z = \sum_{j \neq i} J_{i,j} \left( S_i^x S_j^y - S_i^y S_j^x \right) dT.$$
 (18)

Here  $dW^z \equiv dW^z(T)$  is a Wiener increment such that  $\langle dW^z(T)dW^z(T)\rangle = dT$  and  $\langle dW^z(T)\rangle = 0$  (ref. 59). To properly model the experiment, we directly use coupling matrices  $J_{i,j}$  as characterized in our platform for all calculations; see, for example, Fig. 1b. We average our results over  $5 \times 10^3$  trajectories, which we find to be sufficient to obtain a sampling error well within the size of experimental error bars.

## Effect of global dephasing on spin squeezing

We can numerically examine the effect of varying levels of global dephasing on our spin dynamics. In Extended Data Fig. 2, we plot the minimum spin-squeezing parameter attainable with varying amounts of global dephasing, ranging from the ideal case of  $\Gamma_z = 0$ to the value of  $\Gamma_z$  obtained from the measured  $T_2$  coherence time in our platform. As in the main text, we observe that sufficiently strong global dephasing can lead to a relative degradation of spin squeezing for larger system sizes. However, our calculations for the power-law XY model suggest that even doubling our current coherence time (or, equivalently, doubling the interaction strength) is enough to ensure a squeezing parameter that improves with system size over all ion numbers realizable in our linear chain. By contrast, a power-law Ising model of equivalent range would require a fourfold increase in the coherence time to realize a scalable spin-squeezing parameter over all system sizes considered, as decoherence from global dephasing is compounded by large non-collective effects arising from the finite-ranged potential.

#### Comparisons with an ideal power-law potential

We can also numerically examine the effect of varying interaction ranges on the spin dynamics. In Extended Data Fig. 3, we plot the minimum spin-squeezing parameter attainable for various interaction ranges, characterized by the power-law exponent  $\alpha$  in the coupling  $J_{i,j} = J_0 |i - j|^{-\alpha}$ . In contrast to our analysis in the main text and in Extended Data Fig. 2, here we directly simulate the dynamics under an ideal power-law interaction, as opposed to the experimentally characterized interaction matrix. This enables us to investigate a wide range of  $\alpha$ . Generally, we observe that the XY model for sufficiently long-ranged interactions enables the generation of spin squeezing at a level comparable with the OAT model for all  $\alpha \lesssim 1$  over all N shown, although we note that systematic offsets from this ideal squeezing at smaller N is an artefact of our numerical approximation for this model. For  $\alpha = 1.2$ , the spin squeezing remains very close to the corresponding OAT solution, with a more pronounced difference observed for  $\alpha = 1.5$ . However, all interaction ranges demonstrate a continued scaling of the spin-squeezing parameter at rates comparable with OAT for all N shown.

By comparison, the analytical results for the power-law Ising model reveal a sensitive dependence on the interaction range, with even the long-ranged case of  $\alpha=0.5$  failing to fully recover the level of spin squeezing in the corresponding OAT model. Furthermore, for the shorter interaction ranges, the spin squeezing seems to gradually trend towards a plateau at larger N, indicating the loss of scalability even in the absence of decoherence.

In regards to our results in the main text, we note that both the experimental and the simulated results for the spin-squeezing dynamics show slight deviations from the OAT model in terms of the minimum spin squeezing. Even though the characterized  $J_{i,j}$  in Fig. 1b approximates a power law with  $\alpha \approx 1$ , the tails of the measured potential demonstrate a reduction compared with this ideal power law. Thus, the discrepancy in the observed spin squeezing compared with the OAT model can be understood as a consequence of the shorter-ranged potential in our platform compared with an ideal power law.

## Structure factor and linear spin-waves

In Fig. 2, we study the dynamics of the structure factor (equation (5)), which can be recast into a form that can be directly measured in the experiment

$$\langle \hat{C}_{k} \rangle = \frac{1}{2N} \sum_{i < j} \langle \hat{\sigma}_{i}^{y} \hat{\sigma}_{j}^{y} + \hat{\sigma}_{i}^{z} \hat{\sigma}_{j}^{z} \rangle \cos(k(r_{i} - r_{j}))$$

$$-\frac{1}{2N} \sum_{i} \langle \hat{\sigma}_{i}^{x} \rangle + \frac{1}{2}.$$
(19)

In particular, at short timescales, the structure factor can be used to estimate the occupation of linear SWE. Using the Holstein–Primakoff approximation, we can map spin operators into quadratures written in terms of bosonic annihilation and creation operators  $\hat{b_i}$  and  $\hat{b_i}$ . In the linear spin-wave approximation, we have

$$\hat{\sigma}_i^X = 1 - 2\hat{b}_i^{\dagger} \hat{b}_i \tag{20}$$

$$\hat{\sigma}_i^y \simeq -i(\hat{b}_i - \hat{b}_i^{\dagger}) \tag{21}$$

$$\hat{\sigma}_i^z \simeq -(\hat{b_i} + \hat{b_i}^{\dagger}). \tag{22}$$

The linear approximation is valid if  $\langle \hat{\sigma}_i^x \rangle \lesssim 1$ , that is, the spins remain primarily polarized along the x-axis. The initial CSS polarized along +x maps to the bosonic vacuum state and the dynamical evolution under equation (4) describes the generation of SWE in terms of these bosonic fields.

In momentum space, the bosonic operators are given by  $\hat{b}_k = \sum_i e^{-ikr_i} \hat{b}_i / \sqrt{N}$ , in which  $r_i$  is the location of ion i in the chain. We wish to study the occupation  $\langle \hat{n}_k \rangle = \langle \hat{b}_k^{\dagger} \hat{b}_k \rangle$  of the different modes with momentum k. The mode occupation can be approximated in terms of the structure factor that is measured in the experiment

$$\frac{\langle \hat{n}_{+k} \rangle + \langle \hat{n}_{-k} \rangle}{2} \simeq \langle \hat{C}_k \rangle. \tag{23}$$

The slow, finite growth of the  $k \neq 0$  structure-factor component, that is, the zero-mode occupation of the linear spin-wave in the OAT model, is an artefact arising from the onset of non-Gaussian correlations at times beyond about 2 ms, which are neglected in the linear SWE. Note that there exist alternative approaches to estimate SWE using experimentally measured data<sup>60,61</sup>. However, these methods are not applicable to highly non-collective models, such as the Ising model. Therefore, we rely on the structure factor to emphasize the distinction between our TFI model and a pure Ising model.

## **Data availability**

The experimental data generated and analysed during this study are available in the Zenodo repository, https://doi.org/10.5281/zenodo.8124375.

## **Code availability**

The code used for simulations in this study is available from the corresponding author on reasonable request.

- Joshi, M. K. et al. Observing emergent hydrodynamics in a long-range quantum magnet. Science 376, 720–724 (2022).
- Zhu, S.-L., Monroe, C. & Duan, L.-M. Trapped ion quantum computation with transverse phonon modes. *Phys. Rev. Lett.* 97, 050505 (2006).
- Wu, C. F. J. Jackknife, bootstrap and other resampling methods in regression analysis. Ann. Stat. 14, 1261–1295 (1986).

- Foss-Feig, M., Hazzard, K. R. A., Bollinger, J. J. & Rey, A. M. Nonequilibrium dynamics of arbitrary-range Ising models with decoherence: an exact analytic solution. *Phys. Rev. A* 87, 042101 (2013).
- Schachenmayer, J., Pikovski, A. & Rey, A. M. Many-body quantum spin dynamics with Monte Carlo trajectories on a discrete phase space. Phys. Rev. X 5, 011022 (2015).
- Zhu, B. H., Rey, A. M. & Schachenmayer, J. A generalized phase space approach for solving quantum spin dynamics. New J. Phys. 21, 082001 (2019).
- Huber, J., Rey, A. M. & Rabl, P. Realistic simulations of spin squeezing and cooperative coupling effects in large ensembles of interacting two-level systems. *Phys. Rev. A* 105, 013716 (2022).
- Muleady, S. R., Yang, M., White, S. R. & Rey, A. M. Validating phase-space methods with tensor networks in two-dimensional spin models with power-law interactions. Preprint at https://arxiv.org/abs/2305.17242 (2023).
- 59. Gardiner, C. W. Stochastic Methods: A Handbook for the Natural and Social Sciences 4th edn (ed. Haken, H.) (Springer, 2009).
- Roscilde, T., Comparin, T. & Mezzacapo, F. Entangling dynamics from effective rotor/ spin-wave separation in U(1)-symmetric quantum spin models. Preprint at https://arxiv. org/abs/2302.09271 (2023).
- Roscilde, T., Comparin, T. & Mezzacapo, F. Rotor/spin-wave theory for quantum spin models with U(1) symmetry. Preprint at https://arxiv.org/abs/2303.00380 (2023).

**Acknowledgements** We acknowledge stimulating discussions with members of the LASCEM collaboration about realizing spin squeezing in trapped ions with short-range interactions that initiated the project, as well as valuable feedback on the manuscript by W. Eckner and A. Kaufman. We also acknowledge support by the Austrian Science Fund through the SFB BeyondC (F7110)

and funding by the Institut für Quanteninformation GmbH, by the Simons Collaboration on Ultra-Quantum Matter, which is a grant from the Simons Foundation, and by LASCEM through AFOSR no. 64896-PH-QC. Support is also acknowledged from the AFOSR grants FA9550-18-10319 and FA9550-19-1-0275, by the NSF JILA-PFC PHY-1734006, QLCI OMA-2016244, NSF grant PHY-1820885, by the U.S. Department of Energy, Office of Science, National Quantum Information Science Research Centers, Quantum Systems Accelerator and by NIST.

**Author contributions** The research was devised by S.R.M., M.K.J., R.K., A.M.R. and C.F.R. S.R.M. and A.M.R. developed the theoretical protocols. J.F., M.K.J., F.K., R.B. and C.F.R. contributed to the experimental setup. J.F., M.K.J. and F.K. performed the experiments. M.K.J., J.F. and R.K. analysed the data and S.R.M. carried out numerical simulations. S.R.M., M.K.J., J.F., R.K., A.M.R. and C.F.R. wrote the manuscript. All authors contributed to the discussion of the results and the manuscript.

Competing interests The authors declare no competing interests.

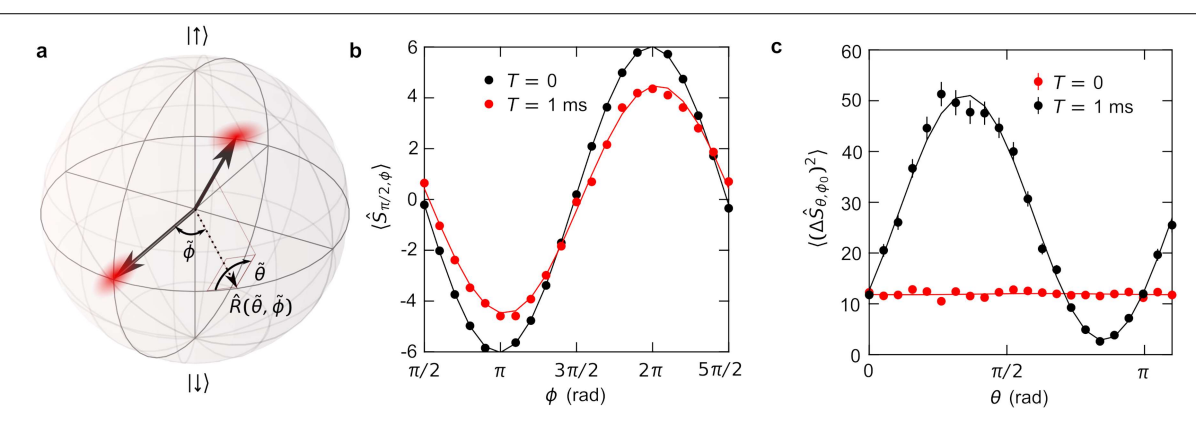
#### Additional information

 $\textbf{Supplementary information} \ The online version contains supplementary material available at \ https://doi.org/10.1038/s41586-023-06472-z.$ 

**Correspondence and requests for materials** should be addressed to Ana Maria Rey or Christian F. Roos.

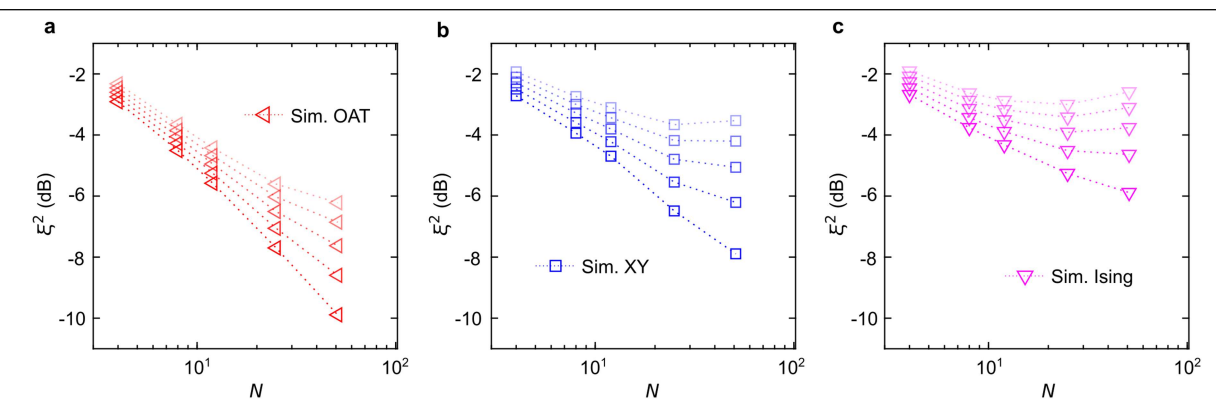
**Peer review information** *Nature* thanks Sebastian Carrasco, Luming Duan, Michael Goerz and the other, anonymous, reviewer(s) for their contribution to the peer review of this work. Peer reviewer reports are available.

Reprints and permissions information is available at http://www.nature.com/reprints.



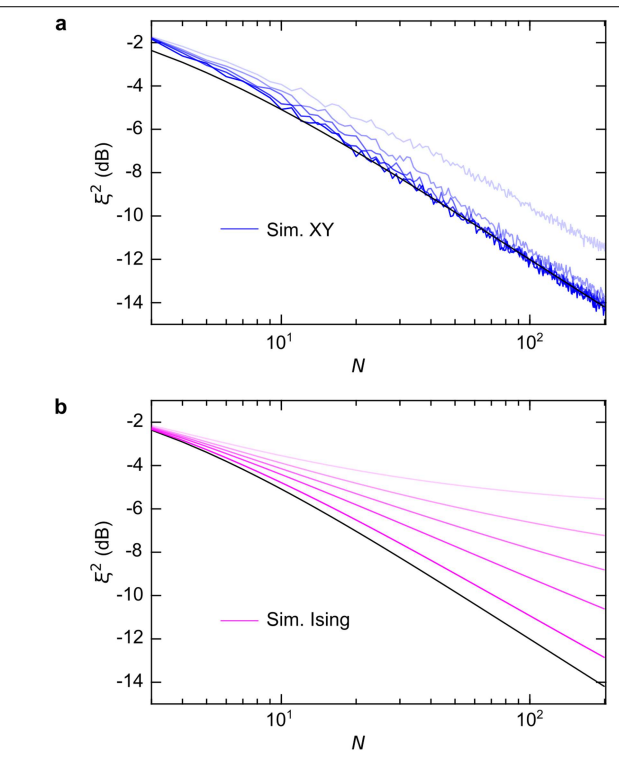
**Extended Data Fig. 1**| **Assessment of the experimentally prepared spin state. a**, The outcome of the entangling interaction on the spins pointing along the x-axis is depicted as a variance ellipse.  $\xi^2$  is evaluated from two sets of measurements that are obtained after a rotation  $\hat{R}(\widetilde{\theta}, \widetilde{\phi})$  has been applied to the state. **b**, Applying  $\hat{R}(\pi/2, \widetilde{\phi})$  for various values of  $\widetilde{\phi}$  allows us to measure the spin projection  $\langle \hat{S}_{\pi/2,\phi} \rangle$  in any direction along the equator. From the sinusoidal

fits (solid lines), we obtain the Bloch vector length and orientation and the angle  $\phi_0$  between the x-axis and the mean spin orientation.  $\mathbf{c}$ , Applying  $\hat{R}(\widetilde{\theta}',\phi_0)$  for various values of  $\theta$  allows us to measure the variance  $\langle (\Delta \hat{S}_{\theta,\phi_0})^2 \rangle$  in any direction orthogonal to the mean spin direction. From the fitted data, we extract the minimal orthogonal variance  $\langle (\Delta \hat{S}_{\mathbf{n}_1})^2 \rangle$  and the angle  $\theta_0$  for which the minimal variance is aligned with the z-axis.



**Extended Data Fig. 2**| **Simulated effect of global dephasing on spin-squeezing preparation.** a, Dependence of  $\xi^2$  on system size, for varying levels of the global dephasing as obtained from analytic calculations of the OAT model with  $\chi = J$ . The opacity of the markers increases with the associated  $T_2$  coherence time, for which we show results for coherence times of 69 ms (lightest),  $2 \times 69$  ms,

 $3\times69$  ms and  $4\times69$  ms, as well as for infinite coherence time (darkest). **b**, Analogous results for numerical calculations of the power-law XY model. **c**, Analytical calculations for the power-law Ising model. We use couplings  $J_{i,j}$  as characterized in our platform for each system size (the dotted lines are a guide to the eye).



Extended Data Fig. 3 | Simulated effect of interaction range on spin-squeezing preparation. a, Dependence of  $\mathcal{E}^2$  on the interaction range, for varying values of the power-law exponent  $\alpha$  obtained from numerical calculations of the XY model in the absence of decoherence. The opacity of the markers increases with the interaction range, for which we show results for  $\alpha=1.5$  (lightest), 1.2, 1.0, 0.8 and 0.5 (darkest). Compared with our analysis elsewhere in the text, in which we use the experimentally characterized  $J_{i,j}$  approximating a power-law potential, here we directly use the ideal power-law interaction  $J_{i,j} = J_0 | i - j |^{-\alpha}$ . We also use the results of simulations through DDTWA without decoherence for all system sizes. The solid black curve indicates the corresponding spin squeezing for an OAT model. b, Analogous results for analytical calculations of the power-law Ising model.